Journal Name

ARTICLE

Surface Heterogeneity and Inhomogeneous Broadening of Vibrational Line Profiles

Received 00th January 20xx,
Accepted 00th January 20xx

DOI: 10.1039/x0xx00000x

www.rsc.org/

Skandar Taj, Diane Baird, Alexander Rosu-Finsen* and Martin R. S. McCoustra

The surface heterogeneity of amorphous silica ($aSiO_2$) has been probed using coverage dependent temperature programmed desorption (TPD) of a simple probe molecule, carbon monoxide (CO). The resulting distribution of interaction energies is the foundation from which an environmentally broadened vibrational line profile synthesis has been undertaken. These simulations are compared with measured line profiles recorded at 0.1 cm^{-1} resolution using reflection-absorption infrared spectroscopy (RAIRS). A comparison of such line profile synthesis for CO on amorphous silica and on porous amorphous solid water (p-ASW) is also reported and conclusions are drawn as to the vibrational relaxation and surface dynamics of the CO molecule on the two surfaces.

Introduction

Vibrational spectroscopy is a powerful family of techniques for the characterisation of molecules in a wide range of environments.[1] The vibrational spectra of molecules in condensed phases are sensitive to the local environment in which the molecules find themselves. Both vibrational frequencies and line profiles reflect that sensitivity.

Vibrational frequencies shift reflecting changes in both force fields, because of intermolecular interaction induced changes in electron density distributions around vibrational chromophores, and mass distributions. Over the years, many empirical correlations have been established reflecting the impact of environment on vibrations for both chromophores in isolated molecules,[2] as exemplified by the carbonyl C=O chromophore,[3] and chromophores in molecular clusters, especially hydrogen-bonded systems.[4]

Fermi's Golden Rule and the energy–time Uncertainty Principle ultimately govern vibrational line profiles, like those of other spectroscopic transitions, and yield symmetric Lorentzian profiles for vibrational transitions in isolated molecules.[5] Efficient non-radiative mechanisms reduce vibrational excited state lifetimes and hence homogeneously, and symmetrically, broaden linewidths often resulting in Gaussian or Voigt line profiles. In the gas phase, temperature (average molecular speed – Doppler Broadening) and pressure (collision frequency – Pressure Broadening) are the principle broadening mechanisms resulting in homogeneous broadening of gas phase line profiles.[6] On solid surfaces, molecular translation and rotation are frustrated and weakly interacting adsorbates on simple ionic solids can therefore exhibit relatively narrow linewidths. The classic example of this is found in the work of Ewing and co-workers.[7,8] These authors estimate the natural linewidth for the vibration of carbon monoxide (CO) on the NaCl (100) surface at 5 K to be of the order of 10^{-8} cm^{-1}, and suggest that the observed linewidth, 0.07 cm^{-1}, results from the residual heterogeneity of the NaCl surface.[7,8] In contrast, on metal surfaces, vibrating dipoles couple with the free electrons in the metal band structure providing a fast and efficient mechanism for relaxing excited adsorbate vibrations *via* electron-hole pair creation.[9,10] The resulting line profiles are broad, for example varying from around 5 to 15 cm^{-1} for CO on metal single crystal surfaces, and asymmetric, reflecting Fano coupling between the adsorbate vibration and the non-adiabatic electron-hole pair continuum of the substrate.[11,12] Additionally, these systems, as with halide surfaces, are often subject to further broadening due to environmental heterogeneity.[13] Environmental heterogeneity reaches its extreme with the profiles of vibrational lines of adsorbates interacting with supported metal and metal oxide catalysts.[14]

As illustrated by the few examples above, it is the clear that CO is a very sensitive environmental probe. However, its utility as such extends far beyond Earth-bound laboratories with its widespread use in remotely probing both the gas phase and solid state in astrophysical environments.[15-18] This is nicely illustrated by a combination of observation[16] and experiment[19] that has tentatively identified CO directly bound to silicate surfaces in some cold, dense environments.

Recently, a combination of vibrational spectroscopy at cryogenic temperatures and computational investigations has permitted the derivation of a vibrational frequency – interaction energy correlation for CO in a variety of cluster and surface bound environments.[20] The linear X…CO interaction particularly shows a strong linear correlation,

$$\Delta\bar{\upsilon} \,/\, \mathrm{cm}^{-1} = 3.330\left(E_b \,/\, \mathrm{kJ\ mol}^{-1}\right) + 2.308 \qquad (1)$$

between the vibrational wavenumber shift, $\Delta\bar{\upsilon}$, from the isolated CO vibrational wavenumber and the strength of the interaction experienced by the CO molecule in a particular environment, E_b. This nicely illustrates the sensitivity of the vibrational frequency of the CO molecule in the linear configuration to its interaction in complexes and on surfaces where the interactions are predominantly non-covalent in nature.

Thus, in systems demonstrating environmental heterogeneity where the strength of the interaction, or distribution of strengths, is

Address: Institute of Chemical Sciences, Heriot-Watt University, EDINBURGH, EH14 4AS, UK.
**Author to whom correspondence should be directed: ar163@hw.ac.uk*

known, the frequency shift(s) could be predicted and the CO vibrational line profile synthesised. This paper will demonstrate the feasibility of such environmentally broadened vibrational line profile synthesis from a knowledge of relevant environmental interaction energies for the case of CO on amorphous silica ($aSiO_2$). The relevant interaction energies will be recovered from inversion of temperature programmed desorption (TPD) data as illustrated in reference [19]. In addition, in synthesising line profiles, this analysis should reveal something of the vibrational relaxation and surface dynamics of the CO molecule on $aSiO_2$ and so begin to explain the temperature invariant rather asymmetric line shape of the CO vibration reported in reference [19].

Experimental

The experiments were conducted in an ultrahigh vacuum system described in detail previously.[21,22] Briefly, the central 30 cm diameter stainless steel chamber is pumped by a liquid nitrogen trapped diffusion pump (Edwards, EO6) backed by a mechanical rotary pump (Edwards, E2M18) to a base pressure of 2×10^{-10} mbar after baking. The oxygen-free high-conductivity (OFHC) copper sample block is coated with **a 300 nm thick** $aSiO_2$ **film** deposited by electron-beam evaporation of fused silica[23] is mounted onto the end of a closed-cycle helium cryostat (APD, CH-202). The silica substrate is heated by a cartridge heater (Heatwave Labs, Inc.) embedded in the OFHC copper substrate and surface temperatures are monitored using a KP (Gold-Chromel) thermocouple. The chamber is equipped with a line-of-sight quadrupole mass spectrometer (Hiden Analytical Ltd, HAL301) for TPD and FTIR spectrometer (Varian 670-IR) and associated optics for RAIRS.

CO (CK Special Gases Ltd., 99.997% purity) and H_2O (Fluka, 99.9% purity) was deposited by background dosing onto the $aSiO_2$ substrate held at 18 K, **at which all experiments were conducted**. Exposures of the sample to the gas are expressed in monolayer (ML) estimated from the corresponding exposure assuming unit sticking probability. TPD is performed by applying a heating ramp of 0.1 – 0.5 K s^{-1} to a suitable final surface temperature. Desorbing species were detected using the quadrupole mass spectrometer (QMS). **Consecutive TPD experiments, from 0.2 to 1 ML, were conducted on the same day. Build-up of gas-phase CO or de-gassing of CO from the chamber walls is considered negligible due to the limited overall daily dose of 3 ML. Further to this, the QMS monitored CO dosing (m/z = 12, 14 and 28) to verify the purity of CO. A line-of-sight housing around the QMS ensured that the TPD data was collected only from the heated substrate.** RAIR spectra were measured at a 75° angle incidence to the normal of the surface; the infrared radiation being collected by a MCT detector cooled with liquid nitrogen. Spectra were recorded at an instrument-limited resolution of 0.1 cm^{-1} by co-addition of 512 scans at the base temperature of the UHV system.

Results and Discussion

CO on Amorphous Silica

Figure 1 presents a RAIR spectrum of 0.6 ML CO on $aSiO_2$ at 18 K in the sub-monolayer regime. The line profile is clearly asymmetric with typical full-width-at-half-maximum (FWHM) of 5.6 cm^{-1}; considerably larger than the 0.1 cm^{-1} instrument-limited resolution used in recording the spectra. As there is no fundamental reason for an asymmetric profile on an insulator surface such as $aSiO_2$, the observed line profiles must be determined by a combination of

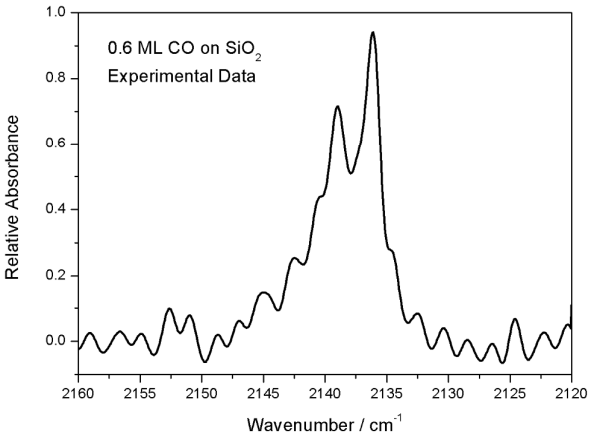

Figure 1: Baselined RAIR spectrum of 0.6 ML CO on $aSiO_2$.

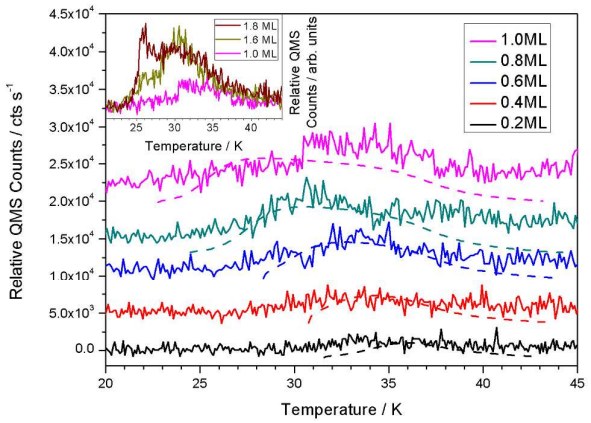

Figure 2: TPD data for sub-monolayer quantities of CO desorbing from $aSiO_2$ as a function of the indicated exposures in monolayers recorded on m/z = 12 m_u. The individual TPD traces have been offset for clarity with the dashed lines relating to TPD simulations. The insert contains the sub-monolayer to multilayer transition for CO on $aSiO_2$.

environmental heterogeneity in addition to homogeneous broadening associated with relaxation of the excited CO vibration through its weak mechanical coupling with the vibrations of the $aSiO_2$ substrate.

The TPD data for CO desorbing from $aSiO_2$ are shown in Figure 2 and exhibit coincident trailing edges at low exposures and a common leading edge at higher exposures **as shown in the insert**. **The dashed lines are the results of sub-monolayer E_{des} simulations based on a previously used FORTRAN 90 model[24], the use and relevance of this model will be discussed later in this section.** The **data in the insert** is consistent with multilayer growth **as seen from the clear shift in the leading edge of desorption. This** allows us to identify the exposure necessary to generate a monolayer coverage on the $aSiO_2$ surface, which **is estimated to contain 2.88 × 10^{15} molecules cm^{-2}**. Hence, we can define **CO** surface coverages for all exposures. The coincidence in trailing edges is usually associated with recombinative second-order desorption, however there is no evidence to suggest that CO dissociates on $aSiO_2$ at low temperature. Rather, the $aSiO_2$ surface presents a range of binding sites with different binding energies for adsorption.[25] The trailing edge alignment indicates that the molecules are mobile enough on the $aSiO_2$ surface to find the deepest, energetically most favourable binding sites. Consequently, molecules situated in weaker binding

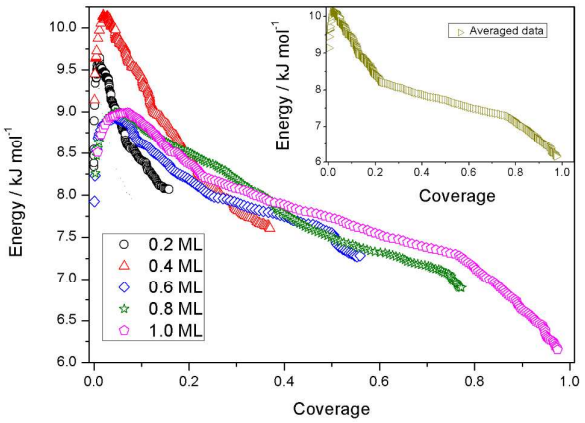

Figure 3: E_{des} as a function of N_{ads}, the surface concentration of adsorbed CO for background dosed sub-monolayers of CO with averaged data in the insert.

sites desorb first, resulting in desorption peak broadening. Since the assumption of a single value for the activation energy of desorption, E_{des}, is no longer valid, direct inversion of the Polanyi–Wigner Equation (2):

$$r_{des} = -\frac{dN_{ads}(t)}{dt} = \upsilon N_{ads}(t)^n e^{-E_{des}/k_B T} \quad (2)$$

where υ is the pre-exponential factor, n and E_{des} the desorption order and energy, k_B the Boltzmann constant and T the surface temperature, can be used to derive E_{des} as function of the surface concentration at time t, $N_{ads}(t)$:

$$E_{des}\big(N_{ads}(t)\big) = -k_B T \ln\left(\frac{\frac{dN_{ads}(t)}{dt}}{\upsilon N_{ads}(t)^n}\right) \quad (3)$$

Tait *et al.*[26] first reported this method and it has been adapted since in studies of small molecule desorption from environmentally heterogeneous surfaces.[19,25] $dN_{ads}(t)/dt$ is simply determined from the QMS count rate as in the high pumping speed regime of TPD, r_{des} is proportional to the measured change in partial pressure of the desorbing CO. Given **that** we are considering first order desorption in an adsorption system dominated by van der Waals interactions, n and υ are 1 and 1×10^{12} s^{-1}, respectively. The values of $N_{ads}(t)$ were determined by subtracting the total gas phase concentration at the previous time step from the initial surface concentration, N_{tot}. N_{tot} is equal to the rate of bombardment, Z_w, multiplied by the dosing time, τ, (4):

$$N_{tot} = Z_w \tau = \frac{PS\tau}{\sqrt{2\pi m k_B T}} \quad (4)$$

where P is the pressure (in Pascal), S the sticking coefficient and m the mass of a single CO molecule (in kg). At the low surface temperatures employed in this study, desorption is negligible and all molecules are assumed to stick to the surface. Hence, S is 1.

A summary of the experimental results can be seen in Table 1. The range of E_{des} values decrease with increasing coverage as expected and illustrated in the literature.[19,27] The uncertainty related to the desorption energy stems from the uncertainty in the temperature measurements (± 0.5 K). FWHM measurements of each coverage are shown as estimated from the baselined RAIR spectra where the uncertainty is due to the resolution of the FT-IR spectrometer (±0.1 cm^{-1}). The linewidth is calculated from the

CO Coverage / ML	E_{des} / kJ mol^{-1} (± 0.5)	FWHM / cm^{-1} (± 0.1)	δ / cm^{-1} (± 0.05)
0.2	8.1 – 9.6	5.0	2.1
0.4	7.6 – 10.2	5.4	2.3
0.6	7.3 – 8.9	5.6	2.5
0.8	6.9 – 9.0	6.5	2.8
1.0	6.2 – 9.0	6.7	2.9

Table 1: This table shows the experimental values extracted from the TPD and RAIRS experiments of the various CO coverages. δ are the linewidths of the νCO features.

FWHM as stated in Equation 8, however this will be discussed in further detail later in this work. Further to this, the integrated absorption scales linearly with each coverage in the sub-monolayer regime as might be expected from the Beer-Lambert law.

Plots of E_{des} against $N_{ads}(t)$ are constructed for each sub-monolayer CO dose (Figure 3) **from the experimental data presented in Figure 2 along with Equations 2, 3 and 4**. A full analysis involving models of the experimental CO data have previously been detailed for the substrate used in this work[19] and other $aSiO_2$ surfaces.[27] **The averaged data as seen in the insert in Figure 3 will be used from hereon as a representation of the distribution of interaction energies of CO molecules with the $aSiO_2$ surface. Our basis for saying this can be seen when returning to Figure 2. Here, the dashed lines are the results of sub-monolayer desorption simulations where the coverage dependant E_{des} from the insert in Figure 3 is used in the simulation of all our TPD measurements. As can be seen in Figure 2, the data and simulations are consistent and shift toward lower temperature as the coverage increases. This is as expected, when wetting molecules transition from sub-monolayer, to monolayer and on to multilayers. With this said, we use the averaged E_{des} distribution from Figure 3 to derive** the likelihood of **CO** adsorption at a particular site with a given E_{des} ***i.e.*, the value of** $P(E_{des})$.$P(E_{des})$ is given by (5):

$$P(E_{des}) = -\frac{dN_{ads}}{dE_{des}} \quad (5)$$

Figure 4 shows $P(E_{des})$ *versus* E_{des} for the CO-$aSiO_2$ system under consideration. The distribution recovered is not dissimilar to those reported for CO and other small molecules on a number of heterogeneous surfaces.[19,25,26,278,29] Clearly, Figure 4 defines the range of interaction energies associated with the surface heterogeneity on the $aSiO_2$ surface. However, it also gives us the

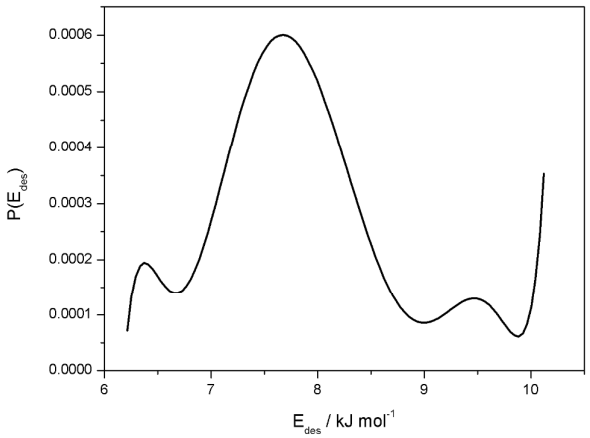

Figure 4: $P(E_{des})$ *versus* E_{des} as derived from sub-monolayer TPD of CO from our $aSiO_2$ substrate.

weighting factor associated with each of those energies, *i.e.* the probability that a CO molecule landing randomly on the $aSiO_2$ surface will find itself in such an environment. Figure 4 is thus central to the simulation of the CO vibrational line profile in this heterogeneous environment.

The line profile synthesis itself is a relatively simple process as outlined in the sequence below;

(1) E_b in equation (1) is equated with E_{des} and the wavenumber shifts, $\Delta\bar{\upsilon}(E_{des})$, calculated for the relevant range of E_{des};

(2) The CO vibrational line positions, $\bar{\upsilon}(E_{des})$, are calculated at each E_{des} according to (6)

$$\bar{\upsilon}(E_{des}) = \bar{\upsilon}_0 + \Delta\bar{\upsilon}(E_{des}) \quad (6)$$

where $\bar{\upsilon}_0$ is the vibrational origin and can be thought of as representing the vibrational wavenumber of CO on non-interacting $aSiO_2$ surface, *i.e.* it encompasses the effect of the mass of the silica surface on the CO vibration;

(3) The vibrational line intensity at each line position, $I(\bar{\nu}, E_{des})$, is calculated assuming a simple Gaussian line profile (7) due to thermal broadening;

$$I(\bar{\upsilon}) = I_0 \sum_{E_{des}} P(E_{des}) e^{-[\bar{\nu}-\bar{\upsilon}(E_{des})]^2/2\delta^2} \quad (7)$$

where δ controls the width of the Gaussian shape (sometimes referred to as the Gaussian RMS width) and is related to the FWHM according to (8)

$$FWHM = 2\sqrt{2\ln(2)}\delta \quad (8)$$

and I_0 is simply an intensity scaling factor. The overall line profile is obtained by summing over E_{des}.

(4) The parameters, $\bar{\upsilon}_0$, δ and I_0, are varied until a good reproduction of the experimental line profile is obtained.

Figure 5 compares the simulated CO vibrational line profile on an $aSiO_2$ surface with that obtained experimentally. The best-fit parameters, $\bar{\upsilon}_0$ and δ, are listed in Table 2. Figure 5A shows the effect of the full distribution of interaction energies recovered from the TPD inversion. This would represent the situation where the CO is ballistically deposited, *i.e.* random deposition without subsequent diffusion on the surface ("stick and stop" as it is sometimes referred to). **The model shown in Figure 5A is the best fit given the ballistic deposition conditions and does not fit the data well. The model is made from the full E_{des} distribution from Figure 4 and a simulated linewidth of 2.5 cm^{-1} (compared to the experimental resolution of 0.1 cm^{-1}) which yields a FWHM of 12.5 cm^{-1}.** On the other hand, Figure 5B illustrates the effect of restricting the accessible energies to only the strongest interactions, *i.e.* permitting diffusion of the CO over the $aSiO_2$ surface even at 18 K. This is achieved by introducing an inverse Boltzmann weighting to (7),

$$I(\bar{\upsilon}) = I_0 \sum_{E_{des}} P(E_{des}) e^{-E_{des}/RT} e^{-[\bar{\nu}-\bar{\upsilon}(E_{des})]^2/2\delta^2} \quad (9)$$

such that the strongest interactions are favoured. This latter situation provides a much better reproduction of the experimental data and is consistent with reference [19].

The best-fit FWHM for the vibrational line profile of CO on $aSiO_2$ is 5.9 cm^{-1}, which should be compared with the measured FWHM of 5.6 cm^{-1}. The difference between these quantities and the asymmetry of the line profile clearly arise from the heterogeneity of the $aSiO_2$ surface. The best-fit value, moreover, points to relatively slow vibrational energy redistribution from the CO vibration into the $aSiO_2$ phonon bath. This should be contrasted to the situation for CO on porous amorphous solid water (p-ASW); the subject of the next section.

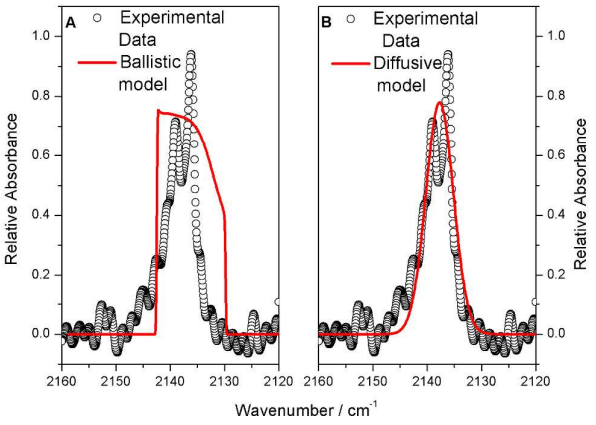

Figure 5: Comparison of the experimental (open circles) and modelled (red line) data of CO on $aSiO_2$. The experimental data is of 0.6 ML CO at 18 K and exhibits a FWHM of 5.6 cm^{-1}. **(A)** shows the simulated line profile when CO is ballistically deposited with a FWHM of 12.5 cm^{-1}. **(B)** shows how a better fit is obtained when CO is free to diffuse using the inverse Boltzmann weighted distribution of E_{des} and leads to a best-fit FWHM of 5.9 cm^{-1}. A point to note is the sub-structure in the experimental line profiles which is due to overlapping features from gas-phase water in the optics purge gas outside of the UHV chamber.

CO on Porous Amorphous Solid Water

To illustrate the generality of the procedure described above, simulations of the vibrational lines profile for CO on p-ASW were undertaken. In approaching this problem, we have utilised the $P(E_{des})$ *versus* E_{des} data of Kay and co-workers.[29] Figure 6 shows the comparison of the experimental and simulated line shapes. It should be noted that the vibrational spectrum of sub-monolayer coverages of CO adsorbed on p-ASW at 20 K exhibits two strong features at 2139 and 2153 cm^{-1}, respectively.[30,31] The 2153 cm^{-1} peak disappearing as the H_2O film is annealed and pore collapse takes place in the p-ASW such that at temperatures above 80 K only

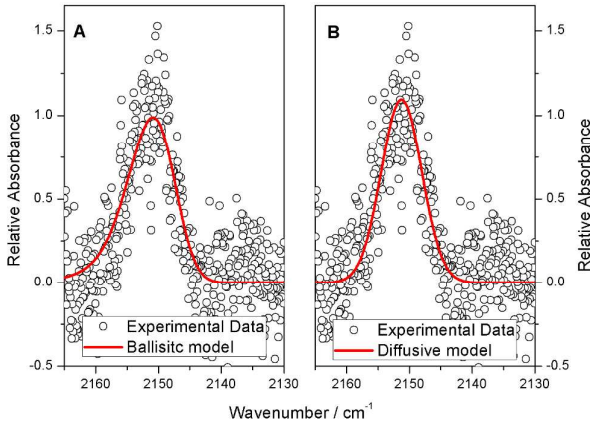

Figure 6: Comparison of the experimental CO stretching band, recorded with the instrument limited resolution, for 5 ML of CO on a p-ASW on our $aSiO_2$ substrate at base temperature (18 K) in UHV with a simulation derived from the data in [20, 29]. **(A)** shows the simulated ballistic line profile for a linewidth of 2.6 cm^{-1} where the experimental data is collected at the instrument limit of 0.1 cm^{-1} and **(B)** is a best-fit diffusive linewidth of 3.2 cm^{-1}.

	$\bar{\upsilon}_0$ / cm^{-1} (± 0.5)	δ / cm^{-1} (± 0.2)	Model FWHM / cm^{-1} (± 0.5)	Exp. FWHM / cm^{-1} (± 0.1)
CO on aSiO$_2$	2075.5	2.5	5.9	5.6
CO on p-ASW (Ballistic)	2108.0	2.6	9.0	8.0
CO on p-ASW (Diffusive)	2089.0	3.2	7.6	8.0

Table 2: Comparison of the best-fit parameters, $\bar{\upsilon}_0$ and δ, and of the corresponding FWHM for the modelled and experimental CO vibrational line profiles on aSiO$_2$ and p-ASW.

the 2139 cm^{-1} band is observed. This leads to the conclusion that the 2153 cm^{-1} feature can be associated with the extended geometry in reference 31, *i.e.* CO adsorbed in a linear configuration with a dangling OH group. While the 2139 cm^{-1} band is attributed to the compact geometry, *i.e.* CO lying parallel to an OH group and perhaps interacting with more than one OH group. The contribution of this latter feature has been subtracted from the data presented in Figure 6 to allow clearer comparison with the environmental heterogeneity simulations of the profile. The best-fit parameters, $\bar{\upsilon}_0$ and δ, derived from the simulation are listed in Table 2.

Figure 6 shows the ballistic deposition and diffusive models as compared to the experimental data. This could indicate that CO is free to both hit-and-stick and diffuse at the same time. Comparing E_{des} values for CO on aSiO$_2$ (6 – 12 kJ mol^{-1}) and CO on p-ASW (11 – 16 kJ mol^{-1})[29] indicates that CO is more strongly bound to the water surface. A widely accepted rule of thumb says that the barrier to surface diffusion is of the order of 10 – 15% of the system's E_{des}[32]. This leads to CO being freer to diffuse on aSiO$_2$ as compared to p-ASW, which can also be understood from Figure 5 and 6. Recent work[33-35] suggests that CO is relatively free to diffuse while about 10% CO molecules on p-ASW can be trapped in pores. This is also seen in Figure 6 as both a ballistic deposition model and a diffusive model fit the experimental data. From the experiments and data presented in this work, an amount of CO trapped or mobile cannot be estimated. However, while developing our thoughts from references [33 – 35] we suggest a diffusive model represents the experimental data to a better degree considering the FWHM as shown in Table 2.

The rather broader FWHM reported in Table 2 is also consistent with a more efficient vibrational relaxation mechanism. It is well known that there is a significant density of vibrational states in p-ASW around 2000 to 2400 cm^{-1} associated with bulk ASW.[36,37] Interaction of the vibrational excited CO *via* a dangling OH bond would therefore provide a very direct route into a phonon bath that is absent in the case of aSiO$_2$.

Conclusions

In concluding this work, it is clear that a relatively simple, and generalizable, procedure can be used to synthesise the vibrational line profiles of CO in an environmentally heterogeneous surface adsorption system where the interactions between the CO and the substrate are dominated by weak, non-covalent interactions. The key requirement for such a synthesis is knowledge of the range of interaction energies and their weighting as encompassed by the $P(E_{des})$ *versus* E_{des} utilised in this simulations. While these data were derived experimentally in the present work, there is no reason, in principle, why similar distributions derived from high quality computational chemistry could not be used. The challenge in that situation would be in identifying both the size of the system to computational model that would accurately reproduce the $P(E_{des})$ *versus* E_{des} data and the most cost-effective computational method to apply to that system.

In simulating these line profiles, we have also highlighted key differences in the vibrational relaxation (p-ASW is more effective than aSiO$_2$) and surface dynamics (CO is **to a certain extent** locked in place on p-ASW but free to diffuse on aSiO$_2$ at 18 K) in these systems that contribute to our growing knowledge of the behaviour of CO on insulator surfaces.

Could this idea be itself inverted to derive $P(E_{des})$ *versus* E_{des} information in systems? That is a challenging question. Logically with sufficient quality in the IR data, it might be possible to assume a functional form for $P(E_{des})$ *versus* E_{des} and iteratively fit synthesised vibrational line profiles to observations using standard least squares minimisation tools. Whether the results of such a fit are robust remains the issue.

Acknowledgements

The authors thank B. D. Kay and R. S. Smith for access to their P(E$_{des}$) versus E$_{des}$ data for CO on porous amorphous solid water. The authors acknowledge the support of the UK Science and Technology Facilities Council (STFC, ST/M001075/1), the UK Engineering and Physical Science Research Council (EPSRC, EP/D506158/1) and the European Community FP7-ITN Marie-Curie Programme (LASSIE project, grant agreement #238258). TS thanks STFC for a project studentship. ARF thanks HWU for a James Watt Scholarship.

Notes and references

1 J. M. Chalmers and P. R. Griffiths (eds), *Handbook of Vibrational Spectroscopy*, (Wiley, Chichester, 2001).
2 R. M. Badger and S. H. Bauer, *J. Chem. Phys.*, 1937, **5**, 839.
3 G. Horvath, J. Illenyi, L. Pusztay and K. Simon, *Acta Chim. Hung.*, 1987, **124**, 819.
4 G. C. Pimentel and C. H. Sederholm, *J. Chem. Phys.*, 1956, **24**, 639.
5 P. Atkins and R. Friedman, *Molecular Quantum Mechanics, Fourth Edition*, (Oxford University Press, Oxford, 2005) Chapter 6.
6 W. Demtröder, *Laser Spectroscopy*, (Springer-Verlag, Heidelberg, 1982) Chapter 3.
7 H. -C. Chang, C. Noda and G. E. Ewing, *J. Vac. Sci. Technol. A*, 1990, **8**, 2644.
8 H. -C. Chang, D. J. Dai and G. E. Ewing, *J. Chin. Chem. Soc.*, 1995, 42, 317.
9 H. Ueba, *Prog. Surf. Sci.*, 1997, 55, 115.
10 H. Arnold, Prog. *Surf. Sci.*, 2011, 86, 1.
11 J.W. Gadzuk and A.C. Luntz, *Surf. Sci.*, 1984, 144, 429.
12 D.C. Langreth, *Phys. Rev. Lett.*, 1985, **54**, 126.
13 R. Ryberg, *Phys. Rev. B*, 1985, **32**, 2671.
14 J. Ryczkowski, *Catalysis Today*, 2001, **68**, 263.
15 J. E. Chiar, P. A. Gerakines, D. C. B. Whittet, Y. J. Pendleton, A. G. G. M. Tielens, A. J. Adamson and A. C. A. Boogert, *Astrophys. J.*, 1998, **498**, 716.
16 K. M. Pontoppidan, H. J. Fraser, E. Dartois, W. –F. Thi, E. F. van Dishoeck, A. C. A. Boogert, L. d'Hendecourt, A. G. G. M. Tielens and S. E. Bisschop, S. E., *Astron. Astrophys.*, 2003, **408**, 981.
17 H. S. Liszt, *Astron. Astrophys.*, 2007, **476**, 291.
18 W. –F. Thi, E. F. van Dishoeck, K. M. Pontoppidan and E. Dartois, *Mon. Not. Roy. Astron. Soc.*, 2010, **406**, 1409.

19 M.P. Collings, V.L. Frankland, J. Lasne, D. Marchione, A. Rosu-Finsen and M.R.S. McCoustra, *Mon. Not. Roy. Astron. Soc.*, 2015, **449**, 1826.
20 M. P. Collings, J. W. Dever and M. R. S. McCoustra, *Phys. Chem. Chem. Phys.,* 2014, **16**, 3479.
21 H. J. Fraser, M. P. Collings and M. R. S. McCoustra, *Rev. Sci. Instrum.,* 2002, **73**, 2161.
22 V. L. Frankland, A. Rosu-Finsen, J. Lasne, M. P. Collings and M.R.S. McCoustra, *Rev. Sci. Instrum.*, 2015, **86**, 055103.
23 J. D. Thrower, M. P. Collings, F. J. M. Rutten and McCoustra M.R.S., *Mon. Not. Roy. Astron. Soc.*, 2009, **394**, 1510.
24 J. D. Thrower, Ph.D. Thesis, 2009, Heriot-Watt University.
25 J. D. Thrower, M. P. Collings, F. J. M. Rutten and M. R. S. McCoustra, *J. Chem. Phys.*, 2009, **131**, 244711.
26 S. L. Tait, Z. Dohnalek, C. T. Campbell and B. D. Kay, *J. Chem. Phys.*, 2005, **122**, 164707.
27 J. A. Noble, E. Congiu, F. Dulieu and H. J. Fraser, Mon. Not. R. Astron. Soc., 2012, **421**, 768.
28 J. A. Noble, S. Diana and F. Dulieu, *Mon. Not. Roy. Astron. Soc.*, 2015, **454**, 2636.
29 R. S. Smith, R. A. May and B. D. Kay, *J. Phys. Chem. B*, 2016, **120**, 1979.
30 M. P. Collings, J. W. Dever, H. J. Fraser, M. R. S. McCoustra and D. A. Williams, *Astrophys. J.*, 2003, **583**, 1058.
31 M. P. Collings, J. W. Dever, H. J. Fraser and M. R. S. McCoustra, *Astrophys. Space Sci.*, 2003, **285**, 633.
32 J.K. Nørskov, F. Studt, F. Abild-Pedersen and Thomas Bligaard, *Fundamental Concepts in Heterogenous Catalysis* (Wiley, Hoboken, 2014), p. 14.
33 F. Mispelaer, P. Theulé, H. Aouididi, J. Noble, F. Duvernay, G. Danger, P. Roubin, O. Morata, T. Hasegawa, and T. Chiavassa, Astron. Astrophys., 2013, **555**, A13.
34 L. J. Karssemeijer, S. Ioppolo, M. C. van Hemert, A. van der Avoird, M. A. Allodi, G. A. Blake, and H. M. Cuppen, Astrophys. J., 2014, **781**, 16.
35 T. Lauck, L. Karssemeijer, K. Shulenberger, M. Rajappan, K. I. Oberg, and H. M. Cuppen, Astrophys. J., 2015, **801**, 118.
36 W. Hagen, A. G. G. M. Tielens and J. M. Tielens, *Chem. Phys.*, 1981, **56**, 367
37 J. P. Devlin, J. Sadlej and V. Buch, *J. Phys. Chem.*, 2001, **105**, 974

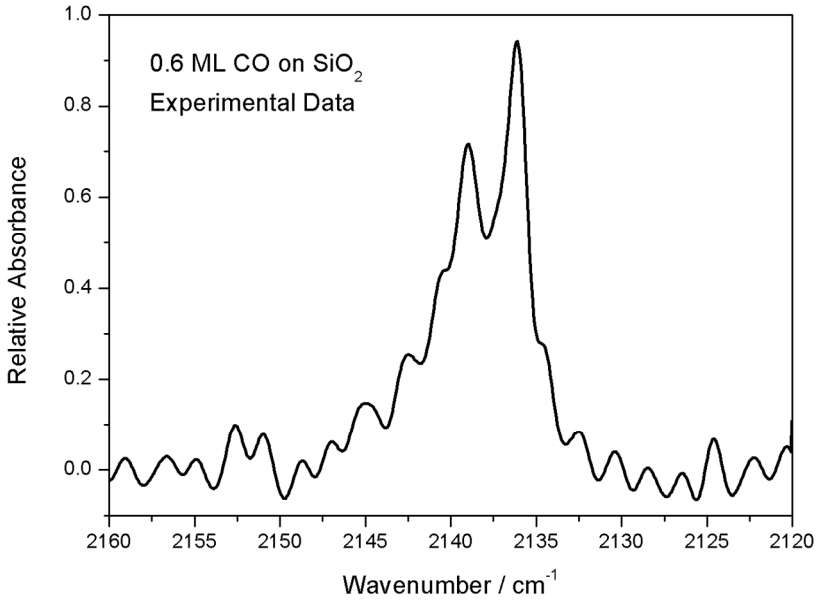

Baselined RAIR spectrum of 0.6 ML CO on $aSiO_2$.

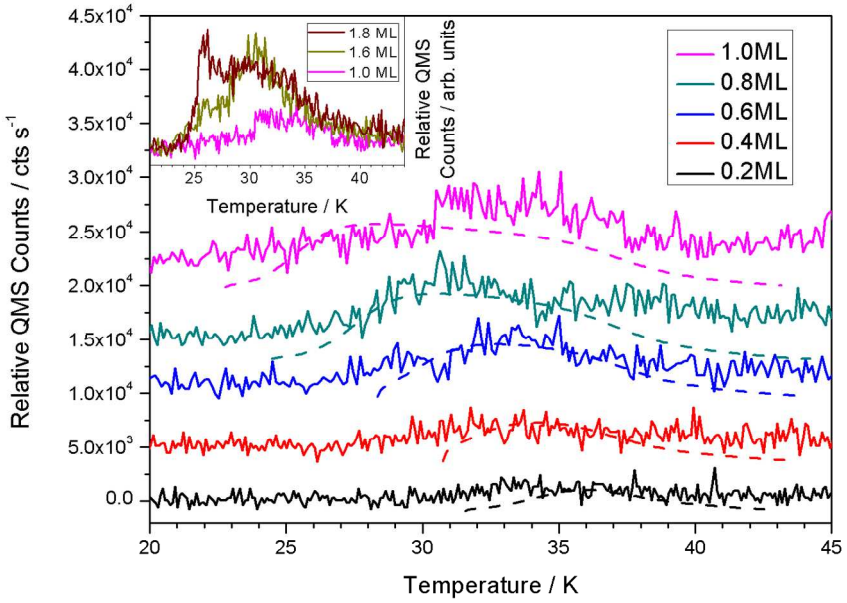

TPD data for sub-monolayer quantities of CO desorbing from $aSiO_2$ as a function of the indicated exposures in monolayers recorded on m/z = 12 m_u. The individual TPD traces have been offset for clarity with the dashed lines relating to TPD simulations. The insert contains the sub-monolayer to multilayer transition for CO on $aSiO_2$.

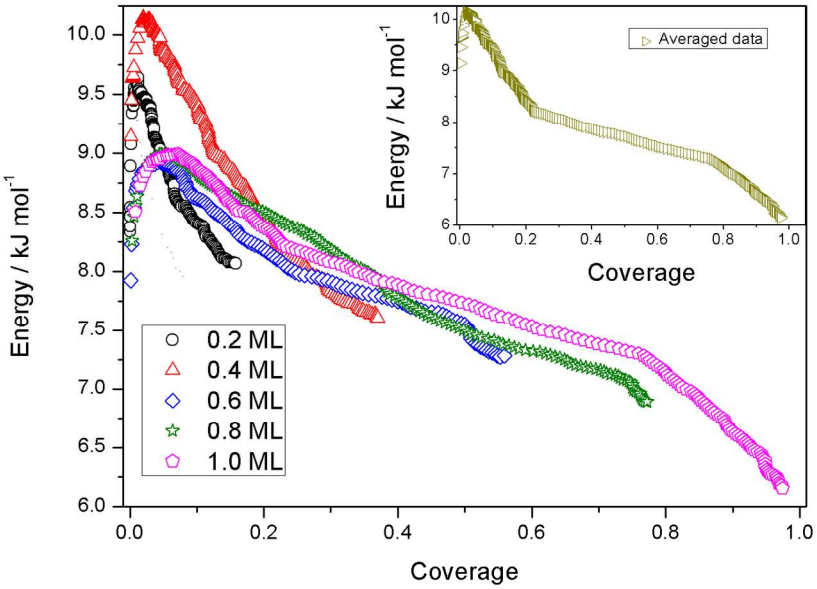

E_{des} as a function of N_{ads}, the surface concentration of adsorbed CO for background dosed sub-monolayers of CO with averaged data in the insert.

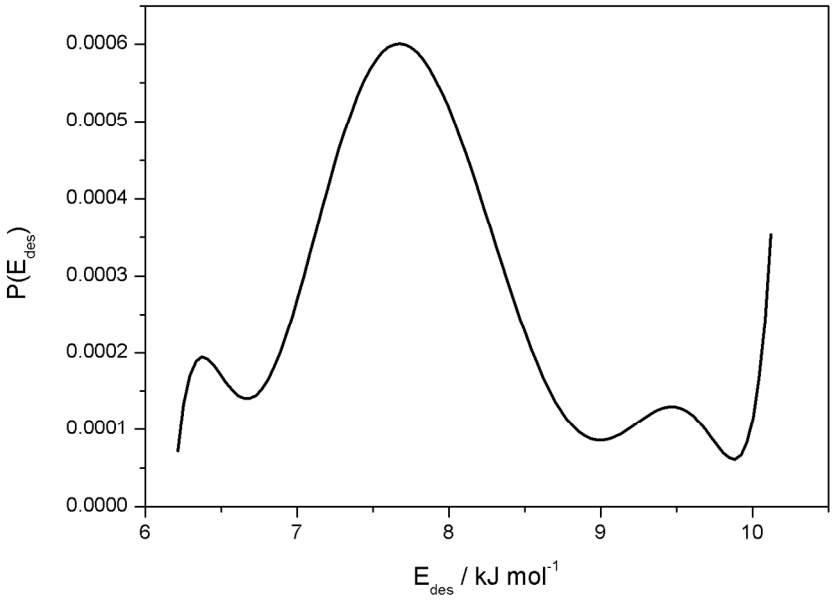

$P(E_{des})$ versus E_{des} as derived from sub-monolayer TPD of CO from our $aSiO_2$ substrate.

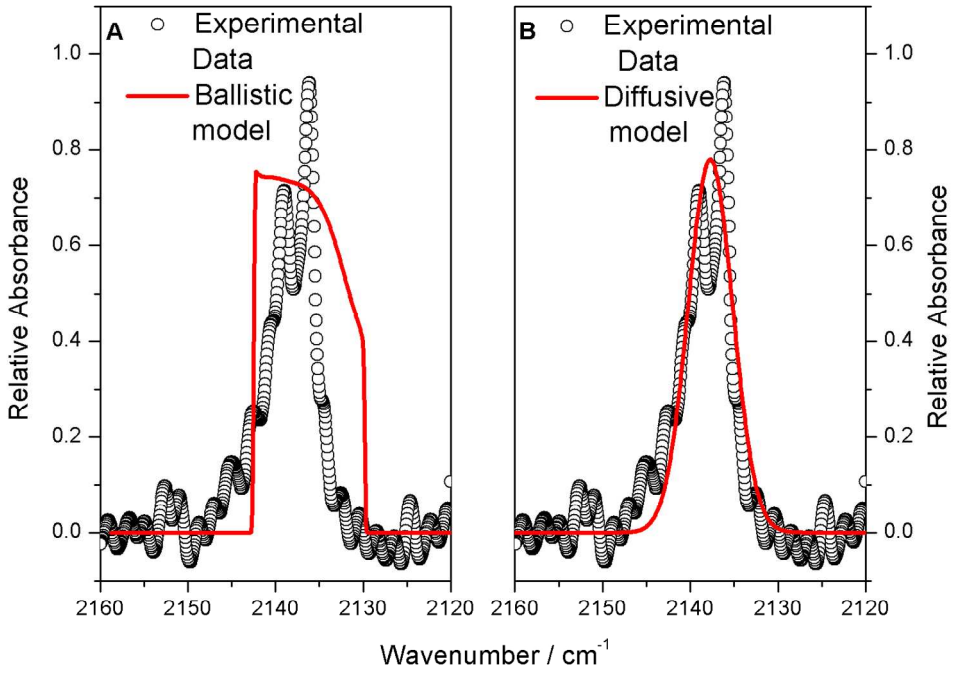

Comparison of the experimental (open circles) and modelled (red line) data of CO on $aSiO_2$. The experimental data is of 0.6 ML CO at 18 K and exhibits a FWHM of 5.6 cm^{-1}. (A) shows the simulated line profile when CO is ballistically deposited with a FWHM of 12.5 cm^{-1}. (B) shows how a better fit is obtained when CO is free to diffuse using the inverse Boltzmann weighted distribution of E_{des} and leads to a best-fit FWHM of 5.9 cm^{-1}. A point to note is the sub-structure in the experimental line profiles which is due to overlapping features from gas-phase water in the optics purge gas outside of the UHV chamber.

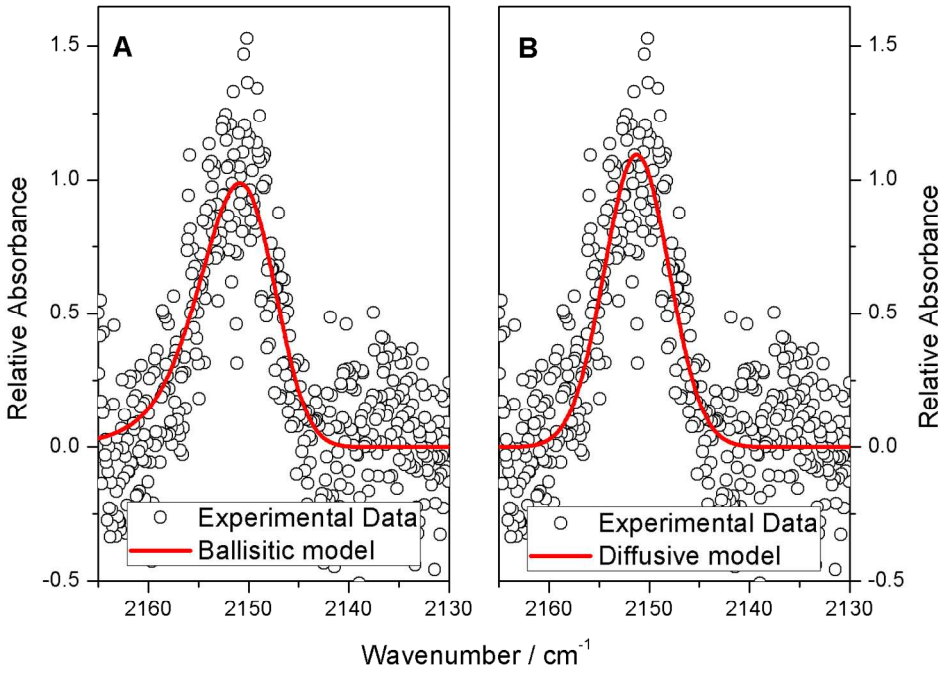

Comparison of the experimental CO stretching band, recorded with the instrument limited resolution, for 5 ML of CO on a p-ASW on our $aSiO_2$ substrate at base temperature (18 K) in UHV with a simulation derived from the data in [20, 29]. (A) shows the simulated ballistic line profile for a linewidth of 2.6 cm^{-1} where the experimental data is collected at the instrument limit of 0.1 cm^{-1} and (B) is a best-fit diffusive linewidth of 3.2 cm^{-1}.